From Order to Chimeras: Unraveling Dynamic Patterns in Active Fluids with Nonlinear Growth

Joydeep Das,[*] Abhishek Chaudhuri,[†] and Sudeshna Sinha[‡]

Department of Physical Sciences,
Indian Institute of Science Education and Research Mohali
Sector 81, SAS Nagar, Punjab 140306, India
(Dated: December 20, 2024)

We explore pattern formation in an active fluid system involving two chemical species that regulate active stress: a fast-diffusing species (A) and a slow-diffusing species (I). The growth of species A is modelled using a nonlinear logistic term. Through linear stability analysis, we derive phase diagrams illustrating the various dynamical regimes in parameter space. Our findings indicate that an increase in the Péclet number results in the destabilisation of the uniform steady state. In contrast, counter-intuitively, an increase in the nonlinear growth parameter of A actually stabilises the homogeneous steady-state regime. Additionally, we observe that greater asymmetry between the species leads to three distinct dynamical phases, while low asymmetry fails to produce oscillatory instability. Numerical simulations conducted in instability regimes show patterns that range from irregular, arrhythmic configurations at high Péclet numbers to both transient and robust symmetry-breaking chimera states. Notably, these chimera patterns are more prevalent in the oscillatory instability regime, and our stability analysis indicates that this regime is the most extensive for high nonlinear growth parameters and moderately high Péclet numbers. Further, we also find soliton-like structures where aggregations of species A merge, and new aggregations spontaneously emerge, and these patterns are prevalent in the phase of stationary instability. Overall, our study illustrates that a diverse array of patterns can emerge in active matter influenced by nonlinear growth in a chemical species, with chimeras being particularly dominant when the nonlinear growth parameter is elevated.

I. Introduction

Pattern formation is a ubiquitous phenomenon in natural systems. In particular, it is an integral part of the development of biological systems. The classical framework for modelling and understanding pattern formation is that of reaction-diffusion systems [1–5]. The emergent patterns observed in this broad class of systems include time-independent and time-dependent oscillatory patterns [1], symmetry-breaking instabilities [6], traveling waves [7], spirals [8] and jumping oscillations [9]. Importantly, many of these patterns have been verified in experiments as well [10, 11].

However, in most biological systems, active transport and forces play a critical role in pattern formation. A prototypical approach to understanding pattern formation in biological systems, therefore, integrates the contributions of mechanical and chemical effects [12], for instance actin networks showing non-equilibrium dynamics by force generation through myosin motor activity [13–15] and pattern formation in active fluid medium in the presence of diffusing chemical species that are advected by self-generated flows produced by concentration-dependent active stress gradients [13, 16]. Specifically, the actomyosin cortex, which lies just beneath the cell membrane, consists of actin filaments and myosin motor proteins which crosslink the actin. This generates mechanical forces, giving rise to an active stress component in a thin mesoscopic layer of the actomyosin cortex. The actomyosin cortex is treated as an active fluid at developmental time scales. The active stress can now be considered to be a function of the concentrations of regulatory chemical species to complete the mechanochemical integration, leading to pattern formation even in the absence of chemical reactions [16]. When extended to two chemical species which undergo advection-diffusion and regulate the active stress, this framework gives rise to pulsatory patterns [13]. Spontaneously emerging localized states in the active fluid medium have led to the understanding of localized cellular patterns [17]. It has been shown that localized states can emerge spontaneously (analogous to isolated clusters of actin and signalling molecules in cancer cells [18]) if the assembly of active matter is regulated by the presence of chemical species that are advected with flows resulting from active stress gradients.

In another research direction, in the context of dynamical systems in general, a class of patterns that have generated intense research interest are chimera states. Broadly, a chimera state is one where a system spontaneously breaks the underlying symmetry and splits into co-existing groups that have very different dynamical features [19–22]. This fascinating phenomenon has been observed in a variety of systems, ranging from Josephson junction arrays [23] to uni-hemispheric sleep in certain animals [24], as well as in continuous media models [25, 26]. Importantly, these chimera states have also been observed experimentally in optical analogs of coupled map lattices [27], Belousov-Zhabotinsky chemical

---
[*] mp21022@iisermohali.ac.in
[†] abhishek@iisermohali.ac.in
[‡] sudeshna@iisermohali.ac.in

oscillator systems [28], two populations of mechanical metronomes [29], electronic circuit systems [30, 31], neurodynamics [32] and Liquid Crystal Light Valve experiments with optical feedback [33]. So it is of immense interest to uncover chimera patterns in different classes of systems in order to gauge the generality of this interesting spatiotemporal pattern.

Motivated by these broad ideas, in this paper, we show the emergence of chimera states in an active fluid with two chemical species regulating the active stress as in Ref. [13], with one species showing a logistic growth. A logistic growth term has been used extensively in many mathematical models of biological systems and provides a very general description of population growth. In particular, a logistic growth model with long-range interactions serves as a generic minimal model for competition for common resources and pattern formation in excited media [34]. In the chemotaxis model, the logistic term is often used to model the growth of cell density [35]. In autochemotactic pattern formation, it is used to model the death and reproduction of self-propelled bacteria [36]. Further, the logistic functional form has been used in an experimentally motivated model of the coupling between reaction-diffusion and active matter [37], as well as in gene expression dynamics [38, 39]. Polymerization in actin gels and solutions is also expressed by a reactive logistic term, useful to describe many characteristic states of actin-wave formation: spots, spirals, and travelling waves [40, 41].

Our central questions in this work are two-fold: First, is nonlinearity detrimental to the stability of homogeneous steady-state states in these active fluid systems, or does the nonlinear logistic growth of a chemical species aid the stability of such regular states? Secondly, we seek to determine the classes of spatiotemporal patterns that emerge in the system when the uniform steady-states lose stability. Specifically, we will search for interesting patterns, such as chimeras, in the space of varying parameters, including the strength of the logistic growth term. That is, we will seek to identify the generic conditions that underlie the transient or robust generation of chimera-like patterns in active fluids. This study then will potentially lead to a better understanding of the effects of the nonlinear growth of a chemical species on emergent dynamical patterns in the active fluid medium and has the scope to motivate engineered in-vitro experiments of reaction-diffusion and active matter systems [37, 42–49].

In the Sections below, we will first describe the model and then present the stability analysis of the system. We will then explore the emergent patterns through numerical simulations over a wide range of parameters. In particular, we will demonstrate the existence of chimera states, solitonic defects and merging-emerging patterns.

II. Mathematical Model

Consider two distinct chemical species (A, I) regulating the active stress in a one-dimensional active fluid medium in a thin-film geometry. The quantities of interest are the concentration fields of $A(x, t)$ and $I(x, t)$ at time t and position x. The evolution equations of the two chemical species in one-dimension are given as:

$$\partial_t A = -\partial_x(vA) + D\partial_x^2 A + rA(1 - A/K) \quad (1)$$
$$\partial_t I = -\partial_x(vI) + \alpha D\partial_x^2 I \quad (2)$$

Thus, both species undergo advection and diffusion, with the diffusive component determined by the diffusion coefficient D and the advective component given by the bulk fluid flow velocity v. The relative diffusion coefficient of the two species is determined by the parameter $\alpha > 0$. The nonlinear logistic growth term, with strength r, is a generic reaction term that has the capacity to destabilize a steady state with zero concentration and also saturates at a finite carrying capacity K. For the active fluid at low Reynolds numbers, the inertial terms can be neglected, and the force balance equation gives

$$\partial_x \sigma = \gamma v, \quad (3)$$

with

$$\sigma = \eta \partial_x v + \sigma_a \quad (4)$$

giving the total stress. σ consists of a viscous stress component $\eta \partial_x v$ with η being the viscosity of the medium and an active stress component σ_a regulated by the concentrations of the chemical species:

$$\sigma_a = \sigma_0 f(A, I) \quad (5)$$

where σ_0 is an active stress amplitude. $f(A, I)$ is a dimensionless function describing the regulations of the active stress:

$$f(A, I) = (1 + \beta)\frac{A}{A + A_S} + (1 - \beta)\frac{I}{I + I_S} \quad (6)$$

where β is an asymmetry parameter, and A_S and I_S represent the saturation values of the concentrations of the two chemical species [13]. For $\beta < -1$, A down-regulate and I up-regulates active stress; for $-1 \leq \beta \leq 1$ both species up-regulates stress and for $\beta > 1$, A up-regulates while I down-regulates active stress.

For further analysis, Eqs.(1)-(4) are expressed in dimensionless form:

$$\partial_t A = -\partial_x(vA) + D\partial_x^2 A + RA(1 - A) \quad (7)$$
$$\partial_t I = -\partial_x(vI) + \alpha \partial_x^2 I \quad (8)$$
$$\partial_x^2 v + Pe\partial_x f(A, I) = v \quad (9)$$

where A, I, x, t and v are now nondimensional and the scaled non-linear growth parameter $R = r\eta/\gamma D$ and the dimensionless Péclet number $Pe = \sigma_0/\gamma D$.

III. Stability Analysis

We consider perturbations to the homogeneous steady state (A_0, I_0) of the form $A = A_0 + A_p(x,t)$, $I = I_0 + I_p(x,t)$ and $v = v_0 + v_p(x,t)$, where, $A_p(x,t) = \delta A_0 e^{\lambda t + ikx}$, $I_p(x,t) = \delta I_0 e^{\lambda t + ikx}$, $v_p(x,t) = \delta v_0 e^{\lambda t + ikx}$. The important parameters here are (1) the Péclet number, which gives the ratio of the advective time scale and the diffusive time scale, (2) the parameter R, which reflects the strength of nonlinearity, and (3) β, which reflects the asymmetry in the two chemical species and influences evolution through the function f. Linear stability analysis of Eqs. (7)-(9), yields the following Jacobian:

$$J = -k^2 \begin{pmatrix} 1 & 0 \\ 0 & \alpha \end{pmatrix} + R(1 - 2A_0) \begin{pmatrix} 1 & 0 \\ 0 & 0 \end{pmatrix}$$
$$+ \frac{Pek^2}{(1+k^2)} \begin{pmatrix} A_0 f_A & A_0 f_I \\ I_0 f_A & I_0 f_I \end{pmatrix} \tag{10}$$

where f_A, f_I are the partial derivatives of f with respect to A and I respectively, evaluated at the homogeneous steady state. In what follows we choose $(A_S, I_S) = (3A_0, 3I_0)$. For each value of wave number $k = \frac{2\pi n}{L}$, $n = 0, 1, \dots$ (considering periodic boundary conditions), we obtain two eigenvalues, which determine the stability and nature of the emergent dynamical pattern. The trace and the determinant of the Jacobian are given as:

$$Tr(J) = -k^2(1+\alpha) - R + \frac{Pek^2(f_A + f_I)}{(1+k^2)} \tag{11}$$

$$\Delta(J) = k^4 \left[\alpha - \frac{Pe(\alpha f_A + f_I)}{(1+k^2)} \right]$$
$$+ Rk^2 \left[\alpha - \frac{Pef_I}{(1+k^2)} \right]. \tag{12}$$

For the functional form given in Eq. 6, evaluating the partial derivatives at the steady state, we obtain $f_A = (1 + \beta)\frac{A_S}{(A+A_S)^2} = \frac{3}{16}(1+\beta)$ and $f_I = (1 - \beta)\frac{I_S}{(I+I_S)^2} = \frac{3}{16}(1-\beta)$. So f_A is always positive, while f_I is negative for $\beta > 1$, and positive for $\beta < 1$. Further notice that for $k \sim 0$, $Tr(J) \sim -R$, and for large k it is negative as well. However, for intermediate k it may be positive for certain parameter values, with the maximum value of $Tr(J)$ occurring at $k_{max}^2 = \sqrt{\frac{3Pe}{8(1+\alpha)}} - 1$ (for $Pe > 8(1+\alpha)/3$). For instance, for $\alpha = 0.1$, this implies that the maximum of the sum of the eigenvalues occurs around $k_{max} \sim 1$ for $Pe \sim 11.7$.

Now, for a homogeneous steady state to be stable under perturbation, the disturbances from the homogeneous profile must damp exponentially rapidly in time. So the real parts of the eigenvalues for all k should be less than zero, implying that $Tr(J) < 0$ and $\Delta(J) > 0$. In the parameter regime where the uniform steady state is unstable, the real part of at least one of the eigenvalues is positive, leading to the formation of diverse patterns. We denote the regime where the leading eigenvalues may not be imaginary as a stationary instability, in analogy with the terminology used in the Turing model. If the eigenvlaues are imaginary for some values of k, an *oscillatory instability* will emerge.

In Fig. 1, we display the phase diagram in the parameter space of the Péclet number Pe and the scaled nonlinear growth parameter R. The phase diagram is generated considering the variation of the eigenvalues with respect to wave number k, and noting the sign of the real part of the leading eigenvalue. The three distinct dynamical phases, namely the stable homogeneous steady state, the regime of oscillatory instability and the regime of stationary instability, are marked with different colors.

It is apparent from the phase diagram that as the Péclet number increases beyond a critical value, the homogeneous steady state gets destabilized giving way to an oscillatory instability. A set of dispersion curves (a-c) are also displayed along-side the phase diagram. These show the behaviour of the real and imaginary parts of the leading eigenvalue when the Péclet number crosses the critical value, thus illustrating the transition from the stable homogeneous steady state to oscillatory instability. On further increase of the Péclet number, the oscillatory instability changes to a stationary instability.

In contrast, interestingly, the phase diagram also shows that the parameter space occupied by the homogeneous steady state is enlarged under increasing R, i.e. larger nonlinear growth yields enhanced homogeneity, indicating the counter-intuitive stabilizing effect of logistic growth on the dynamics. Further, increasing the magnitude of the nonlinear growth term also increases the parameter region supporting oscillatory states. It is also distinctly evident from Figure 1 that the boundaries between the different dynamical regimes have a linear dependence on the scaled nonlinearity R. The slope of the linear rise of the boundary curve separating the homogeneous steady state and the oscillatory state is gentler than that of the boundary between the stationary instability and oscillatory instability. This implies that the oscillatory state increases most significantly with increasing nonlinear growth.

Specifically, our analysis also yields the boundary curve between the stable homogeneous steady state and the oscillatory instability. Along this boundary curve, the condition $Tr(J) = 0$ should be satisfied. Since k_{max} is close to 1 over a large range of Péclet numbers, we can get an approximate expression for the critical Péclet number Pe_c beyond which instability sets in. Considering the values of β, α, A_0, I_0, A_S and I_S given in the phase diagram, this yields:

$$Pe_c = \frac{16}{3}(1.1 + R) \tag{13}$$

This linear relation is indicated by a line in the phase diagram displayed in Fig. 1, and it is clear that this approximate expression fits results from stability analysis over a large large of R. Since the critical value of the Péclet number increases almost linearly with the scaled nonlinear growth parameter R, it implies that the range
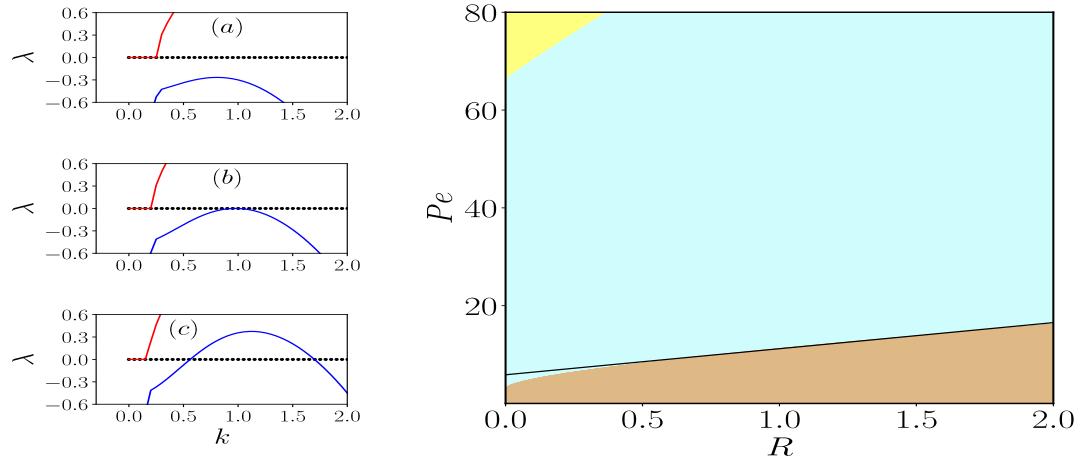
FIG. 1. (Right) Phase diagram of the different dynamical patterns that emerge, in the parameter space of the Péclet number Pe and the scaled nonlinear growth parameter R, obtained from Linear Stability Analysis. Here the ratio of diffusion constants $\alpha = 0.1$ and the asymmetry parameter $\beta = 3$. The brown colour represents the stable homogeneous steady state, pale blue represents oscillatory instability and yellow represents stationary instability. The black curve represents the approximate linear boundary between the stable homogeneous steady state and the regime of oscillatory instability, given by Eqn. 13. Left panels (a),(b) and (c) display the dispersion curves corresponding to $Pe < Pe_c$, $Pe = Pe_c$ and $Pe > Pe_c$ respectively, where $Pe_c = 11.2$ is the critical Péclet number. The blue curve represents the real part of the leading eigenvalue, the red curve represents the imaginary part of the leading eigenvalue, and the black dotted line shows $\lambda = 0$ for reference.
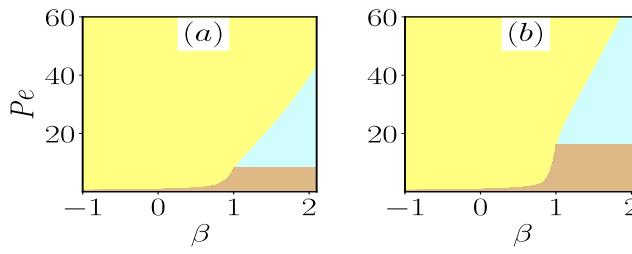

FIG. 2. Phase diagram of the different dynamical patterns that emerge, in the parameter space of the Péclet number Pe and asymmetry parameter β, obtained from Linear Stability Analysis, for $\alpha=0.1$ and scaled nonlinear growth parameter R equal to (a) 0.5 and (b) 2.
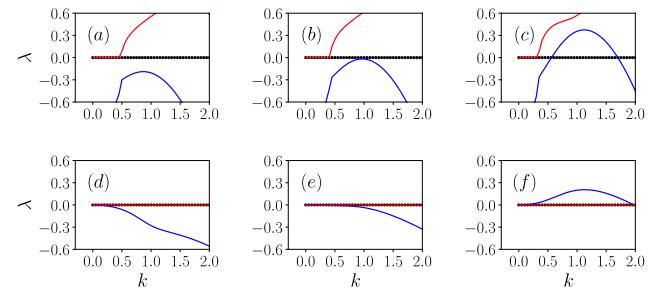

FIG. 3. Dispersion curves obtained from Linear Stability Analysis, for varying Péclet number Pe and asymmetry parameter β. Here $\alpha = 0.1$ and nonlinearity parameter $R = 1$. The first row of panels (a), (b) and (c), corresponding to $Pe < Pe_c$, $Pe = Pe_c$ and $Pe > Pe_c$, show the transition from the stable homogeneous steady state to the oscillatory instability, as Pe increases from 9 to 15, for $\beta = 1.2$. Panels (d), (e) and (f) show the transition from the stable homogeneous steady state to stationary instability as β decreases from 1.1 to 0.7, for fixed Péclet number $Pe = 6$. In all panels the blue curve represents the real part of the leading eigenvalue, the red curve represents the imaginary part of the leading eigenvalue, and the black dotted line shows $\lambda = 0$ for reference.

of Pe over which the homogeneous steady state is stable is directly proportional to R, with larger stable ranges emerging for larger R.

We also observe pattern formation is crucially dependent on the asymmetry parameter β. This is clearly evident from Figure 2, where we display phase diagrams in the parameter space of the Péclet number Pe and asymmetry β for different values of the scaled logistic growth parameter R. When β is low ($\beta < 1$), no regime of oscillatory instability exists for any value of the Péclet number, while for β greater than 1 all three dynamical regimes are possible. Two sets of dispersion curves are also displayed in Fig. 3, showing the behaviour of the real and imaginary parts of the leading eigenvalues when Pe and β cross critical values, underlying different classes of dynamical transitions. In particular, these dispersion curves illus-

trate the transitions from the stable homogeneous steady state to oscillatory instability on increasing Pe, and to the stationary instability on decreasing β. Note that the dependence of the dynamics on the asymmetry β can be rationalized as follows: a negative determinant indicates that the signs of the two eigenvalues are different, and so a negative $\Delta(J)$ cannot yield imaginary eigenvalues (as they necessarily have to be complex conjugates as the
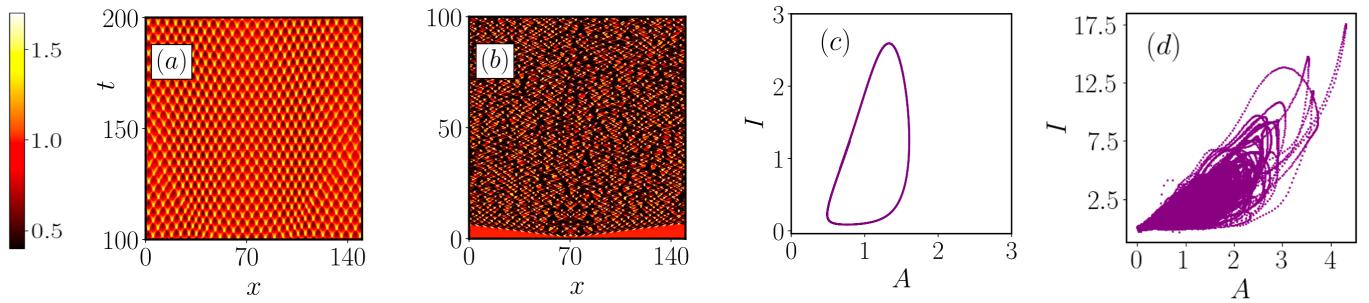
FIG. 4. (Left) Kymographs displaying the evolution of concentration A in time (vertical axis) and space (horizontal axis), for parameter values (a) $Pe = 13$, $\beta = 1.5$, $R = 1$, $\alpha = 0.1$, and (b) $Pe = 48$, $\beta = 3$, $R = 1$, $\alpha = 0.1$. The colors in the heat-map of the concentration A is given by the color-bar that indicates increasing concentrations from $A = 0$ (black) to $A = 2$ (white). (Right) Dynamical attractors in the phase space of $A - I$ concentrations at a typical location in space: (c) Limit Cycle corresponding to the space-time evolution shown in (a), and (d) Chaotic attractor corresponding to the space-time evolution shown in (b).
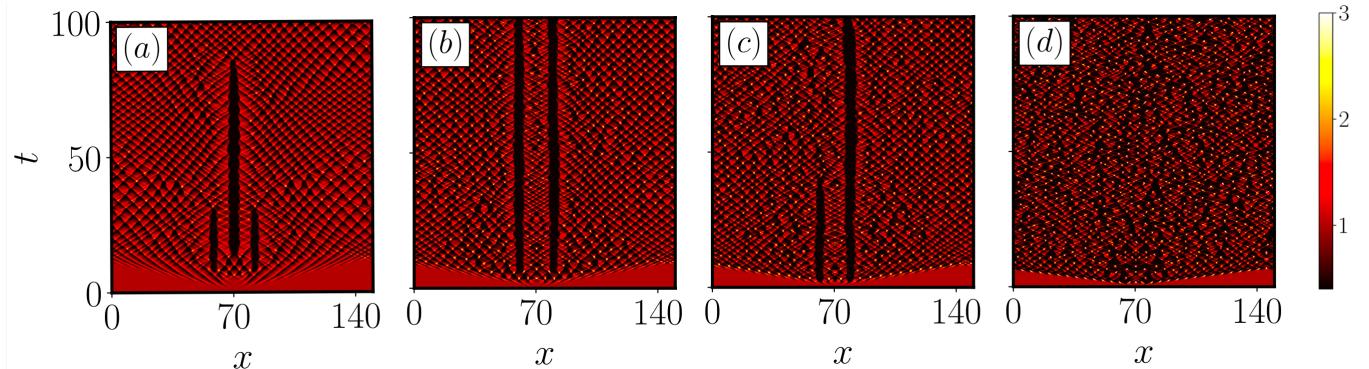

FIG. 5. Emergence of an illustrative sequence of space-time patterns, ranging from transient Chimera states to irregular arrhythmic spatio-temporal patterns, in a system with $R = 1$, $\alpha = 0.1$, $\beta = 3$, for increasing Péclet numbers: (a) $Pe = 27$,(b) $Pe = 35$, (c) $Pe = 39$,(d) $Pe = 48$. Here the heat-map of the concentration A is displayed as a function of time (vertical axis) and space (horizontal axis), with the color bar indicating increasing concentrations from $A = 0$ (black) to $A = 3$ (white).

Jacobian matrix is real). This implies the result that for small α, $\beta > 1$ can yield $\Delta(J) > 0$, and so there can be modes that have oscillatory instability only for $\beta > 1$.

To summarize our results from stability analysis: first, increasing Péclet number leads to the loss of stability of the uniform steady state. Increasing asymmetry β yields three distinct dynamical phases, while low asymmetry does not yield oscillatory instability. Lastly, interestingly, *nonlinear logistic growth aids the stability of the steady state and also enlarges the parameter regime supporting the phase with oscillatory instability.*

IV.   Numerical Simulations

We now explore the spatio-temporal dynamics of the system through extensive numerical simulations over a wide range of parameters. Note that a computational approach is necessary to examine patterns beyond steady states and simple pulsatory or stationary patterns. For instance, spatio-temporal defects and chimera states cannot be gauged by linear stability analysis alone. Fur-

ther, numerical simulations provide valuable verification and consistency checks with analytical results, and they complement the analytical treatment of the system given above.

We solve Eqns. (7)-(9) numerically by using a semi-implicit spectral scheme using periodic boundary conditions. We apply a small localized perturbation to the uniform steady state $(A_0, I_0) = (1, 1)$, with $v = 0$, and follow the system's response to this perturbation. With no loss of generality with respect to the qualitative features, we consider $L = 150$, $\Delta x = L/512$, $\Delta t = 0.0001$. Additionally, We have also examined the dynamics with $\Delta x = L/1024, L/2048$ in order to check the robustness of our qualitative results. Specifically, we will demonstrate that a wide variety of spatiotemporal patterns arise from varying strength of the logistic growth term R, asymmetry β and the Péclet number Pe.

The first key observation is that the homogeneous steady state loses stability as the Péclet number Pe increases beyond a critical value, and this critical value is consistent with that obtained through linear stability analysis. When the homogeneous steady state loses
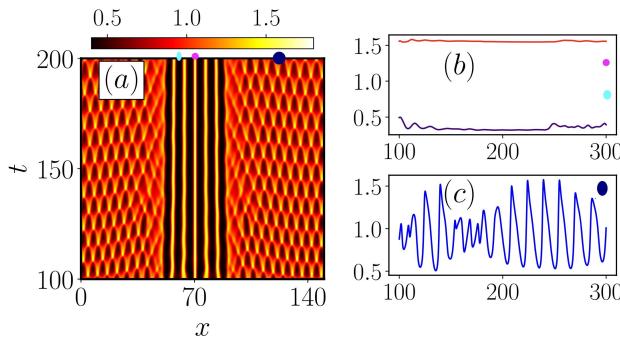
FIG. 6. Long-lived two-regime transient chimera state. The kymograph displays the spatiotemporal pattern formation from time 100 to 200. The panels on the sides display the time evolution of concentration A, at locations in space marked by different symbols in the kymograph. Here the parameters are: $\beta = 1.2$, $\alpha = 0.1$, $R = 1$ and $Pe = 13$.

stability, a range of patterns emerge. Representative examples of these patterns are displayed in Fig. 4. The patterns are characterized through kymographs, namely the heat map of the concentration of species A in space and time (left panels in Fig. 4). Additionally, the temporal evolution at typical locations in space is characterized by dynamical attractors in the phase space of the concentrations of the two chemical species (right panels in Fig. 4). Typically, for smaller Péclet numbers oscillatory states arise, yielding regular limit cycle attractors in phase space. On the other hand, large Péclet numbers give rise to enhanced irregularity in the spatio-temporal patterns. For instance, in the representative examples in the figure, for $Pe = 13$, the emergent space-time patterns are nearly pulsatory, while for $Pe = 48$ one obtains a chaotic attractor.

Fig. 5 shows a representative sequence of space-time patterns that emerge for increasing Péclet numbers beyond the regime of regular pulsatory patterns. This illustrative set of patterns reveals the existence of interesting robust and transient chimera states [50] at moderately high values of the Péclet number. On varying initial states, a wide variety of chimera states emerge. These range from long-lived two-regime chimera states to multi-head transient chimera states that emerge spontaneously at uncorrelated locations and times. The specific patterns that emerge are strongly sensitive to initial states, and the persistence of transient chimeras increases with increasing length-scale L of the system. Representative examples of a transient two-regime chimera state and a three-regime chimera state, are shown in Figures 6-7. In the two-regime chimera state (Fig. 6), two types of patterns coexist. We have homogeneous spatial patches where the concentration is nearly stationary for a significant time, with alternating patches having a high and

low concentration, i.e. nearly homogeneous stationary patches coexist with a spatial region exhibiting oscillatory space-time patterns. In the three-regime chimera state (Fig. 7), nearly homogeneous steady patches coexist with two separate spatial regions exhibiting distinct oscillatory patterns. The time evolution of concentrations at representative locations in the distinct regimes are explicitly shown in Figs. 6-7. Typically, these transient chimera states appear, disappear and re-appear. This sequence repeats over long times before finally terminating and settling down to the asymptotic oscillatory pattern. In the context of transient chimeras, it is interesting to note that cortical chimeras are often transient and identifying them plays a role in predicting epileptic seizures [51].

In parameter regimes beyond the ones supporting chimera states, almost all initial perturbations give rise to irregular arrhythmic oscillatory spatiotemporal patterns, illustrative examples of which are shown in Fig. 4c-d and Fig. 5d. So when the Péclet number is very small, we obtain stable homogeneous steady states. On increasing Pe, chimera states emerge and are found over a considerable range of Péclet numbers. For very high Pe, chimera states again disappear, and irregular arrhythmic patterns, akin to spatiotemporal chaos, are commonly observed. So, one can conclude that a moderately high Péclet number is most conducive to chimera-like states.

In the phase diagrams obtained through stability analysis (cf. Figs. 1-2) , the regime of oscillatory instability is most conducive to chimera states. Notice that this regime is most extensive for large R, implying that the possibility of observing chimeras is enhanced by larger nonlinearity. This connection with the phase diagram is also consistent with the observation of chimeras at moderate Péclet numbers, but not at high Pe where the oscillatory instability gives way to stationary instability. Lastly the asymmetry parameter β needs to be larger than 1 in order to obtain chimeras. This observation is again linked to the fact that the oscillatory instability exists only for $\beta > 1$.

Finally, we observe merging-emerging solitonic structures in the space-time evolution of the concentrations. This class of patterns is illustrated in Fig. 8, which shows the destabilization of the initial near-uniform spatial profile into multi-peak aggregations which evolve through a sequence of emerging and merging events. Such patterns are reminiscent of solitonic defects, where the soliton-like structures emerge, persist for some time and then may disappear, merge with other neighbouring solitonic defects or split into solitonic sub-structures as the system evolves. These patterns are most predominant in the regime of stationary instability. So low asymmetry β and high Péclet numbers are most likely to yield them. Such merging and emerging space-time structures are similar to patterns observed in the dynamics of a model for chemotaxis incorporating a logistic cell growth term [35]. Further, such patterns have also been observed in a model system that mimics nonlinear cell-diffusion [52].
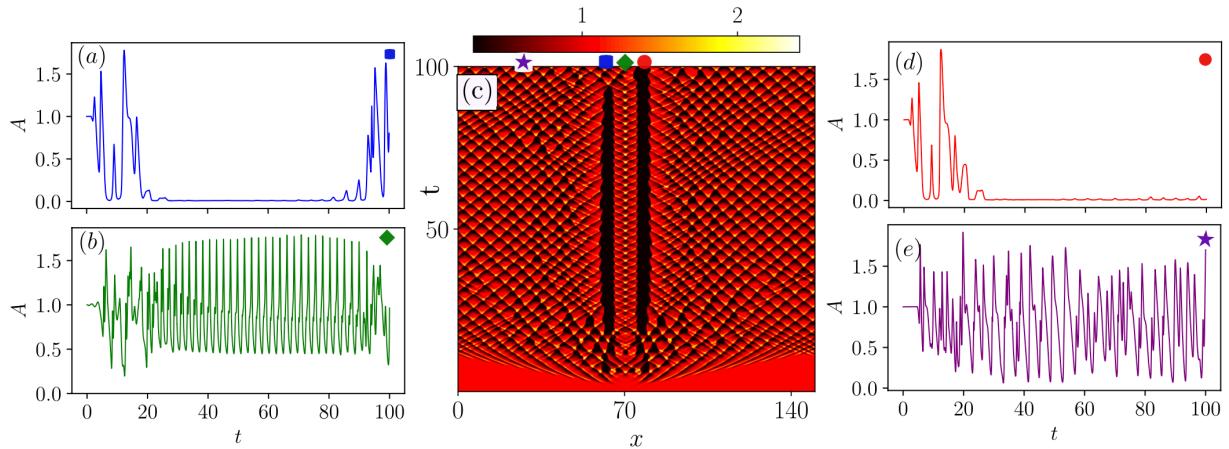
FIG. 7. Three-regime transient chimera state. The kymograph displays the spatiotemporal pattern formation from time 0 to 100. The panels on the sides display the time evolution of concentration A, at locations in space marked by different symbols in the kymograph. Here the parameters are: $\beta = 3$, $\alpha = 0.1$, $R = 1$ and $Pe = 32$.
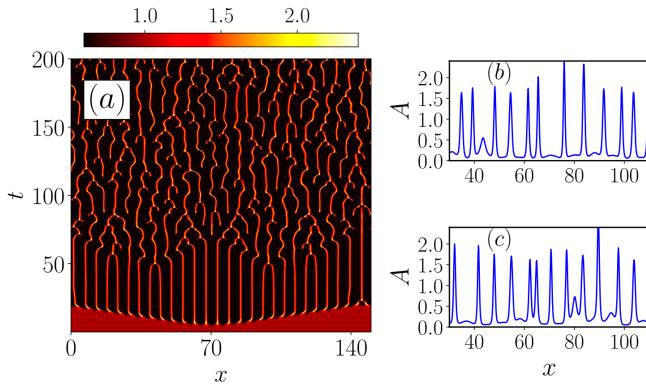

FIG. 8. (a) Kymograph showing Merging-Emerging space-time dynamics, for parameters $Pe = 20$, $R = 1$, $\beta = 1.2$ and $\alpha = 0.1$. The panels (b) and (c) show the spatial variation of concentration A at two instants of time $t = 190$ and $t = 194$. The emergence and annihilation of concentration peaks are clearly visible in the spatial profile.

V. Conclusions

We explored a two component system, where the chemical species interact with the active fluid medium via active stress gradients, and the growth of the fast-diffusing species is modelled by a nonlinear logistic term. We investigated the formation of space-time patterns, both analytically, as well as through extensive numerical simulations. Our key results are summarized below.

First, increasing the Péclet number beyond a critical value leads to the loss of stability of the homogeneous steady state, i.e. instability is induced when the rate of advection is sufficiently greater than the rate of gradient-driven diffusion. Further, the asymmetry of the activator and inhibitor species in our two-component system, as reflected by the parameter β, also has a crucial effect on the emergent dynamical phases. Increasing

asymmetry yields three distinct dynamical phases, while low asymmetry does not yield the oscillatory instability. Lastly, most interestingly, we demonstrate that nonlinear growth aids the stability of the homogeneous steady state. This counter-intuitive phenomenon is evident from the enlarged area of stability of the homogeneous steady state in the phase diagrams, for larger scaled nonlinear growth parameter R. Specifically we also show that the critical Péclet number for the onset of instability rises approximately linearly with R, leading to an expansion of the homogeneous steady state region in parameter space. Our analytical results explicitly showing the emergence of different dynamical phases are completely corroborated by numerical simulations.

The second set of significant results arise in the region of parameter space where the homogeneous steady state loses stability. This region is explored extensively numerically, as well as through the determination of the existence of complex eigenvalues for certain modes in the perturbed system indicating oscillatory instabilities. We find the emergence of diverse classes of patterns in this regime. These range from regular oscillatory space-time patterns, to merging-emerging multi-peak aggregations reminiscent of solitonic defect-like structures, and irregular space-time evolution characterized by chaotic attractors. Most interestingly, we find the emergence of chimera states, both long-lived transient, as well as robust, and these chimeras are predominant in the region of oscillatory instability. Now, the dispersion curves for different modes of the perturbed system obtained through our linear stability analysis show that the region of oscillatory instability is enlarged in the presence of nonlinear growth. This implies the following important result: nonlinear growth enhances the probability of observing chimera states. So these results can potentially aid experimentalists, as they can focus their search for chimera states on classes of systems that are more prone to such patterns.

[1] A. M. Turing, Bulletin of mathematical biology **52**, 153 (1990).

[2] M. Cross and H. Greenside, *Pattern formation and dynamics in nonequilibrium systems* (Cambridge University Press, 2009).

[3] M. C. Cross and P. C. Hohenberg, Reviews of modern physics **65**, 851 (1993).

[4] S. Kondo and T. Miura, science **329**, 1616 (2010).

[5] J. Green and J. Sharpe, Development **142**, 1203 (2015).

[6] I. Prigogine and R. Lefever, The Journal of Chemical Physics **48**, 1695 (1968).

[7] A. Zaikin and A. Zhabotinsky, Nature **225**, 535 (1970).

[8] A. T. Winfree, Science **175**, 634 (1972).

[9] E. Knobloch, H. Uecker, and A. Yochelis, Physical Review E **104**, L062201 (2021).

[10] Q. Ouyang and H. L. Swinney, Nature **352**, 610 (1991).

[11] V. Castets, E. Dulos, J. Boissonade, and P. De Kepper, Physical Review Letters **64**, 2953 (1990).

[12] A. K. Harris, D. Stopak, and P. Warner, Development **80**, 1 (1984).

[13] K. V. Kumar, J. S. Bois, F. Jülicher, and S. W. Grill, Physical review letters **112**, 208101 (2014).

[14] F. Juelicher, K. Kruse, J. Prost, and J.-F. Joanny, Physics Reports **449**, 3 (2007).

[15] S. Ramaswamy, Annu. Rev. Condens. Matter Phys. **1**, 323 (2010).

[16] J. S. Bois, F. Jülicher, and S. W. Grill, Biophysical Journal **100**, 445a (2011).

[17] L. Barberi and K. Kruse, Physical Review Letters **131**, 238401 (2023).

[18] J. Bravo-Cordero, M. Oser, X. Chen, R. Eddy, L. Hodgson, and J. Condeelis, Current Biology **21**, 635 (2011).

[19] Y. Kuramoto and D. Battogtokh, Nonlinear. Phen. Complex. Sys. **5**, 380 (2002).

[20] D. Abrams and S. Strogatz, Phys. Rev. Lett. **93**, 174102 (2004).

[21] S. Sinha, Europhysics Letters , 40004 (2019).

[22] B. K. Bera, D. Ghosh, P. Parmananda, G. Osipov, and S. K. Dana, Chaos: An Interdisciplinary Journal of Nonlinear Science **27** (2017).

[23] K. Wiesenfield, P. Colet, and S. Strogatz, Phys. Rev. Lett. **76**, 404 (1996).

[24] N. Rottenberg, C. Amlaner, and S. Lima, Neurosci. Biobehav. Rev. **24**, 817 (2000).

[25] A. Alvarez-Socorro, M. Clerc, and N. Verschueren, Communications in Nonlinear Science and Numerical Simulation **94**, 105559 (2021).

[26] Z. G. Nicolaou, H. Riecke, and A. E. Motter, Phys. Rev. Lett. **119**, 244101 (2017).

[27] A. Hagerstrom, T. Murphy, R. Roy, P. Hövel, I. Omelechenko, and E. Schöll, Nature Phys. **8**, 658 (2012).

[28] M. Tinsley, S. Nkomo, and K. Showalter, Nature Phys. **8**, 662 (2012).

[29] E. Martens, S. Thutupalli, A. Fourriere, and O. Hallatschek, Proc. Nat. Acad. Sciences **110**, 10563 (2013).

[30] C. Meena, K. Murali, and S. Sinha, International Journal of Bif. & Chaos **26**, 1630023 (2016).

[31] L. Larger, B. Penkovsky, and Y. Maistrenko, Phys. Rev. Lett. **111**, 054103 (2013).

[32] A. Compte, N. Brunel, P. S. Goldman-Rakic, and X.-J. Wang, Cerebral Cortex **10**, 910 (2000).

[33] N. Verschueren, U. Bortolozzo, M. Clerc, and S. Residori, Physical Review Letters **110**, 104101 (2013).

[34] N. M. Shnerb, Physical Review E **69**, 061917 (2004).

[35] K. J. Painter and T. Hillen, Physica D: Nonlinear Phenomena **240**, 363 (2011).

[36] M. Mukherjee and P. Ghosh, Physical Review E **97**, 012413 (2018).

[37] C. del Junco, A. Estevez-Torres, and A. Maitra, Phys. Rev. E **105**, 014602 (2022).

[38] R. A. Fisher, Annals of eugenics **7**, 355 (1937).

[39] Z. Neufeld and E. Hernández-García, *Chemical and biological processes in fluid flows: a dynamical systems approach* (World Scientific, 2009).

[40] X. Yang, D. Marenduzzo, and M. Marchetti, Physical Review E **89**, 012711 (2014).

[41] T. Le Goff, B. Liebchen, and D. Marenduzzo, Physical Review Letters **117**, 238002 (2016).

[42] A. Padirac, T. Fujii, A. Estévez-Torres, and Y. Rondelez, Journal of the American Chemical Society **135**, 14586 (2013).

[43] S. M. Chirieleison, P. B. Allen, Z. B. Simpson, A. D. Ellington, and X. Chen, Nature chemistry **5**, 1000 (2013).

[44] Y. Vyborna, J.-C. Galas, and A. Estevez-Torres, Journal of the American Chemical Society **143**, 20022 (2021).

[45] A. Senoussi, J.-C. Galas, and A. Estevez-Torres, Science Advances **7**, eabi9865 (2021).

[46] A.-D. C. Nguindjel, P. J. de Visser, M. Winkens, and P. A. Korevaar, Physical Chemistry Chemical Physics **24**, 23980 (2022).

[47] M. Zaferani, R. Song, S. Petry, and H. A. Stone, Proceedings of the National Academy of Sciences **121**, e2315992121 (2024).

[48] A. S. Zadorin, Y. Rondelez, J.-C. Galas, and A. Estevez-Torres, Physical review letters **114**, 068301 (2015).

[49] R. Rajasekaran, C.-C. Chang, E. W. Weix, T. M. Galateo, and S. M. Coyle, Cell **187**, 345 (2024).

[50] M. Wolfrum and O. Omel'chenko, Phys. Rev. E **84**, 015201 (2011).

[51] C. Lainscsek, N. Rungratsameetaweemana, S. S. Cash, and T. J. Sejnowski, Chaos: An Interdisciplinary Journal of Nonlinear Science **29** (2019).

[52] Z. Wang and T. Hillen, Chaos: An Interdisciplinary Journal of Nonlinear Science **17** (2007).